AQUA
Water Infrastructure, Ecosystems and Society

IWA PUBLISHING

 AQUA — Water Infrastructure, Ecosystems and Society Vol 72 No 4, 479 doi: 10.2166/aqua.2023.188

Temporal moment-based approach to understand the dissolved-phase LNAPL recovery and associated characteristics in the porous system under dynamic groundwater table conditions

Abhay Guleria[a], Pankaj Kumar Gupta [b,c,d,*], Sumedha Chakma[a] and Brijesh Kumar Yadav[b]

[a] Department of Civil Engineering, Indian Institute of Technology Delhi, Delhi 110016, India
[b] Department of Hydrology, Indian Institute of Technology Roorkee, Roorkee 247667, India
[c] Faculty of Environment, University of Waterloo, Waterloo, ON N2L 3G1, Canada
[d] Indian Institute of Technology (I.I.T.) Delhi, New Delhi, 110 016, India
*Corresponding author. E-mail: pk3gupta@uwaterloo.ca

PKG, 0000-0003-0683-4148

ABSTRACT

The dissolved-phase hydrocarbon recovery can be the first step in decontaminating the soil–water system if spilled with light/dense non-aqueous phase liquid (L/D-NAPL). This study proposes a temporal moment-based approach to investigate the effectiveness of groundwater table manipulations for recovering dissolved-phase byproducts of light non-aqueous phase liquid (LNAPL) from the subsurface system. Temporal moments were computed utilizing experimentally observed and HYDRUS-simulated dissolved-phase toluene concentration data, representative of LNAPL, under stable and dynamic groundwater table fluctuation (GWTF) scenarios. Zeroth temporal moment (ZTM) showed that the hydrocarbon mass recovery varied from 1,804 to 5,190.6 mg/L × h, with the highest variation for the rapid GWTF scenario. An increase in the ZTM of hydrocarbon was observed with an increase in the rate of change of magnitude of the water table and pore velocity fluctuation as in the case of a rapid GWTF as compared to a stable GWTF case. The value of mean residence time for the stable groundwater table case was highest for the entire experimental duration, followed by slow, general, and rapid cases. Temporal moment analysis revealed that the high dissolved-phase hydrocarbon recovery could be achieved by manipulating groundwater table conditions. The present study provides a powerful technique to improve dissolved hydrocarbon remediation in mineral aquifers using hydrological restorations.

Key words: groundwater table, LNAPL, remediation, sand tank experiment, temporal moment analysis, toluene

HIGHLIGHTS

- 2D sand tank experiments were performed under varying subsurface flow conditions.
- The LNAPL recovery increases with water level fluctuation amplitudes.
- Water table manipulation can act as a remediation tool for LNAPL-polluted sites.
- The outcomes will help to advise the remediation and management of polluted sites.

GRAPHICAL ABSTRACT

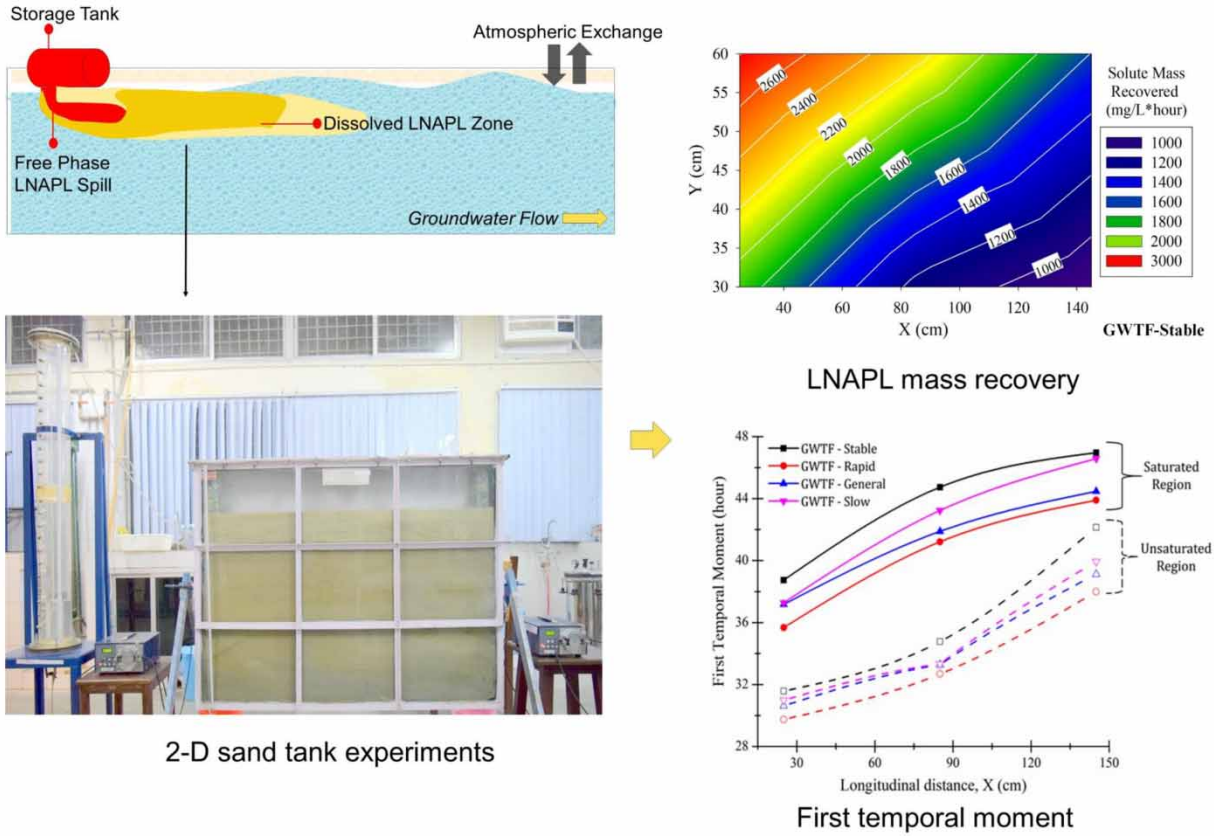

1. INTRODUCTION

Pollution of soil–water resources due to the release of hydrocarbon contaminants is a serious threat to human and ecological health (Garg *et al.* 2015, 2017). Light non-aqueous phase liquids (LNAPLs) have major concerns in the subsurface due to their high sensitivity to varying subsurface conditions, which enable them to spread widely (Kim & Corapcioglu 2003; Oostrom *et al.* 2006). The LNAPLs are not freely miscible in water, but a small quantity of dissolved phase in the soil–water system is sufficient to seriously degrade soil–water quality (Essaid *et al.* 2015; Gupta *et al.* 2019; Gupta & Yadav 2020). Typically, the main sources of these dissolved hydrocarbons are residual mass, either lighter or denser-NAPLs, which may have been spilled in the past and generally occur near fuel production sites and petrol stations (U.S. EPA 2006). The hydrocarbon compounds may start dissolving from residual NAPL with soil moisture in the capillary zone and create a mobile plume, referred to as 'plume' in the manuscript, which subsequently moves to the downgradient locations due to advective flow (Chrysikopoulos 1995; Narayanan *et al.* 1998a, 1998b; Fagerlund *et al.* 2008; Yadav *et al.* 2012). In laboratory-scale conditions, the flow pattern changed from linear to non-linear, even with a gradual increase in the hydraulic gradient (Basack *et al.* 2022). Thus, it is important to understand the fate of plumes thoroughly under varying groundwater flow regimes in order to frame a suitable engineered remediation strategy. A series of two-dimensional (2D) sand tank experiments were performed by Gupta *et al.* (2019) to understand the fate of plumes under four groundwater table conditions. They observed a large plume with varying concentrations (15–200 mg/L) of toluene, a representative hydrocarbon, under rapid groundwater table fluctuation (GWTF), referred to as a rapid case in this manuscript. Their results are also in-line with Gupta & Yadav (2020), wherein they highlighted the dependency of biodegradation on the initial substrate concentrations. They observed degradation increases with an increase in initial concentration of toluene up to 50 ppm and remained maximum till 100 ppm before starting to decrease with an increment in substrate concentration. A low degradation rate at a high substrate concentration shows the toxic effects of pollutants on toluene degraders (Gupta *et al.* 2020). In order to improve treatability, it is necessary to estimate the recovery of dissolved hydrocarbon mass from the high-concentration zone first.

Several mathematical modeling techniques, such as the finite-difference method (FDM) and finite-element method (FEM), were applied to understand the groundwater flow (Beegum *et al.* 2018; Omar *et al.* 2019, 2020, 2021) and contaminant transport in the subsurface system (Šimůnek *et al.* 2016; Guo *et al.* 2019; Ekeleme *et al.* 2021). For example, the analytic element method (AEM) and FDM were used to study the groundwater flow dynamics in the Lower Ganga river basin from 2004 to 2017 (Omar *et al.* 2019). Their study found that the AEM performed better than the FDM for steady-state solutions. However, the FDM was found to be better than AEM in the case of transient modeling and heterogeneous aquifer system. Similarly, the AEM model was integrated with particle swarm optimization (PSO) and compared with the FDM-PSO model in the identification of flow parameters of unknown wells (Gaur *et al.* 2023). Their study found the AEM-PSO model as more effective than the FDM-PSO model. In another study, a loosely coupled SWAT–MODFLOW model was used to study the effects of recharge and abstraction on the groundwater levels of the Nairobi aquifer system (Nyakundi *et al.* 2022). A hybrid SWAT–MODFLOW model was found to be an efficient and realistic approach as it incorporated factors such as land use-land cover, topography, climatic factors, and soil type (Nyakundi *et al.* 2022). Furthermore, moment analysis based on experimental and model-simulated concentration data was found to be an effective approach to studying the flow and contaminant transport behavior in the subsurface system (Govindaraju & Das 2007; Blackmore *et al.* 2018; Guleria *et al.* 2020; Singh *et al.* 2021, 2022).

Temporal moment analysis (TMA) proved to be an effective method to understand the time-averaged response of contaminants like hydrocarbons, in the subsurface system as compared to the conventional way of analyzing breakthrough curves (BTCs) at downgradient location(s) or spatial concentration profile(s) (Pang *et al.* 2003; Govindaraju & Das 2007; Sharma *et al.* 2012; Goltz & Huang 2017). For example, flow and solute transport behavior at site-specific and laboratory-based column conditions was studied based on the temporal moments (Blackmore *et al.* 2014). Also, the relationship between the dispersion coefficient and seepage velocity for the transport of carbon disulfide vapor in the partially saturated 2 m long column was derived based on temporal moments (Kleinknecht *et al.* 2017). The experimental and theoretical data of tracer transport in soil columns under single- and two-phase flow conditions was analyzed based on temporal moments (Singh *et al.* 2021, 2022). On the basis of the temporal moments as output metrics, a comparison of the conventional model with the hybrid mathematical model to analyze the simulation capabilities was made (Guleria *et al.* 2020; Sharma *et al.* 2020). Thus, utilizing observed and physics-based simulated concentration data under various groundwater flow regimes via TMA can be a simple technique for estimating the dissolved hydrocarbon recovery and its associated parameters from plumes.

The experimental data from Gupta *et al.* (2019) were rare and unique, as the fate and transport of LNAPL were simulated under four groundwater table conditions. A question yet to answer is how much-dissolved hydrocarbon can be recovered from such a dynamic subsurface system. Furthermore, the role of groundwater table dynamics on the dissolved hydrocarbon recovery was unclear even after Gupta *et al.* (2019). Gupta *et al.* (2019) analyzed the transport dynamics of the dissolved-phase plume emanating from the LNAPL pool accumulated in a capillary fringe under stable and fluctuating groundwater table conditions based on the BTCs and spatial concentration profiles. In this research, it is estimated how much-dissolved hydrocarbon could be recovered from such a dynamic subsurface system which can help field practitioners and pollution remediation managers. It provides details on the role of groundwater table dynamics on dissolved hydrocarbon recovery and its associated parameters.

2. METHODOLOGY

To understand the role of the groundwater table as a local driver of plume size and spreading, we utilized the data from a 2D sand tank experiment performed by Gupta *et al.* (2019). The 2D sand tank setup having inner dimensions of 150 cm × 120 cm × 10 cm was connected with an auxiliary column containing the collected groundwater (Supplementary material, Figure A1 of Appendix A). The pure-phase toluene was injected from the top surface near the top-left side of the tank at a constant rate of 2 mL/min up to 5 min and allowed to create an LNAPL pool above the water table (WT). There were seven sampling ports, referred to as P1–P7, situated near WT fluctuation zone, and seven sampling ports in the saturated zone, referred to as P8–P14 (Supplementary material, Figure A1 of Appendix A). In the stable case, a constant groundwater flux was applied at the inlet, and the same was extracted at the outlet, hence keeping the location of WT at a constant height. On the other hand, in GWTF cases, i.e., GWTF-Rapid, GWTF-Slow, and GWTF-General, the rise/fall of WT was maintained using a peristaltic pump. A detailed summary of the 2D sand tank experiment is provided in Supplementary material,

Appendix A. In this study, the dissolved-phase experimental and HYDRUS-simulated BTCs of toluene at port numbers 1, 4, and 7 of the unsaturated zone and at port numbers 8, 11, and 14 of the saturated zone (Supplementary material, Figure A1 of Appendix A) from Gupta *et al.* (2019) were used to compute the temporal moments. The schematic of the methodology adopted to compute temporal moments is presented in Figure 1.

For modeling of toluene in the sand tank experimental setup conditions, the Galerkin FEM was used to solve the governing flow and transport equations in HYDRUS-2D software (Šimůnek *et al.* 2006). A 2D numerical domain with dimensions corresponding to those of the sand tank was created for the simulation of soil–water flow and LNAPL transport through the subsurface system. To solve the water flow equation, saturated moisture content was assumed as the initial moisture level, and the top side of the domain was taken as WT boundary condition. No-flux condition was taken for a bottom boundary, while a continuous flux-type boundary with pulse condition was considered at the left and right side of the domain for GWTF cases. In the GWTF-Stable case, influx and outflux boundaries without pulse conditions were assumed. Furthermore, to solve the LNAPL transport equation, zero toluene concentration was assumed as an initial condition for the whole numerical domain. An LNAPL source point was considered at the top-left side of the domain, mimicking the 2D sand tank conditions. To comprehend the LNAPL transport dynamics under various GWTF scenarios, simulations were run for 56 h.

2.1. Calculation of temporal moments

The temporal moment of dissolved-phase contaminant concentrations can provide the time-averaged response of solute within the porous media (Naff 1992; Guleria *et al.* 2020). The first four moments (out of n possible moments), were commonly used to define the central distribution tendency (Govindaraju & Das 2007). For example, the zeroth moment relates to total mass density, and the first moment relates to the arithmetic mean (Pang *et al.* 2003; Guleria *et al.* 2019). In physical meaning, zeroth temporal moment (ZTM) reflects the contaminant mass recovered at a particular location or observation point. Furthermore, the first temporal moment describes the time when half of the injected mass has passed through the observation point or the average time spent by contaminant molecules in the porous system. The second temporal moment represents the variance of the BTC, which provides a measure of the degree of mixing of the mass within the porous system (Govindaraju & Das 2007; Guleria *et al.* 2020). Thus, temporal moments of toluene concentrations (mass recovered, mean residence time) were computed by calculating the absolute temporal moments at a location x before determining the ratio of various absolute temporal moments (Figure 1). The zeroth, first, and second normalized temporal moments were computed using numerical integration in the MATLAB environment. After computing the various temporal moments, correlation analysis between observed and simulated moments was carried out to determine the discrepancies.

The nth order absolute temporal moment at a location x, is defined mathematically by Equation (1) as (Govindaraju & Das 2007):

$$M_n = \int_0^T t^n C(x, t)dt \tag{1}$$

where for $n = 0$, 1, 2, obtained moments M_0, M_1, and M_2 represents zeroth-, first-, and second-order absolute temporal moments, respectively, and T is the total resident time. $C(x, t)$ is the LNAPL dissolved-phase concentration for a particular location x at all the time levels (BTC at location x).

Furthermore, nth order normalized temporal moments are obtained from the following Equations (2)–(3) (Govindaraju & Das 2007):

$$\mu_n = \frac{M_n}{M_0} = \frac{\int_0^T t^n C(x, t)dt}{\int_0^T C(x, t)dt} \tag{2}$$

$$T_1(x) = \mu_1 \tag{3}$$

$$T_2(x) = \mu_2 - (\mu_1)^2 \tag{4}$$

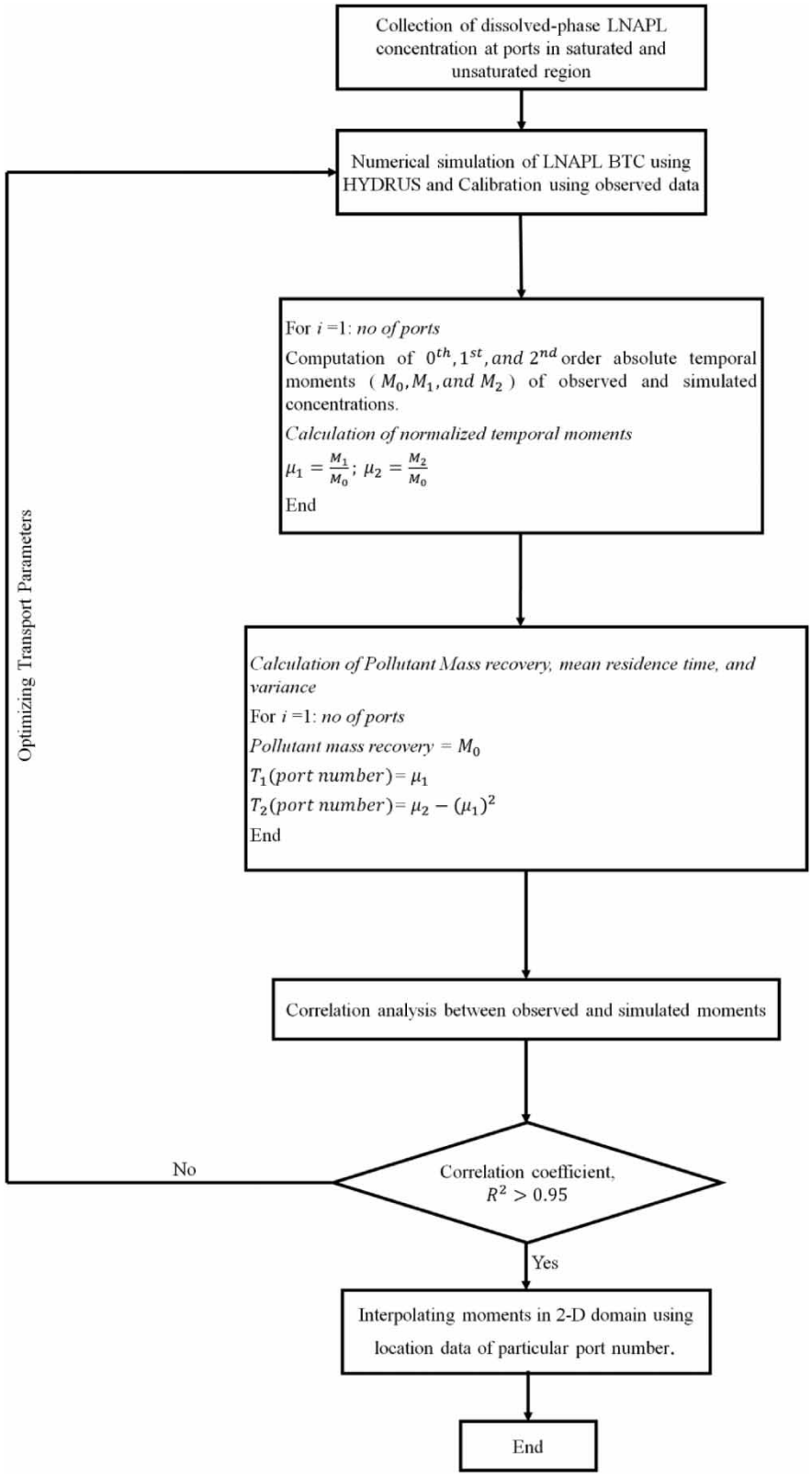

Figure 1 | Schematic of the methodology adopted for moment analysis of LNAPL transport in a 2D sand tank setup.

where μ_1 and μ_2 are the normalized first and second temporal moments, whereas $T_1(x)$ and $T_2(x)$ are the first and second temporal moments.

3. RESULTS AND DISCUSSION

3.1. Toluene mass recovery

The ZTM gives the dissolved-phase toluene mass recovered at a location and was calculated for all the ports in the unsaturated (ports P1, P4, and P7) and deep saturated (ports P8, P11, and P14) regions. Furthermore, spatial distribution of recovered mass is presented using a contour plot for all the GWTF cases, as shown in Figure 2. In the GWTF-Stable case, value of ZTM was found to vary from 837 to 2,806.2 mg/L × h (Figure 2(a)). For the GWTF-Rapid case, ZTM was found to vary from 1,804 to 5,190.6 mg/L × h, with the highest variation of 3,386.6 mg/L × h among all four cases, while for the GWTF-Slow case, ZTM varies from 1,179.4 to 3,516.3 mg/L × h (Figure 2(c)). A high toluene mass recovery was observed under rapidly fluctuating groundwater table conditions. It was also found that the large toluene mass can be recovered from the region interfacing LNAPL pool. The lowest amount of the toluene mass recovery was observed for the GWTF-Stable case, in which WT was maintained at a constant height. The toluene mass recovery was observed highest near the LNAPL source zone, where fluctuation in groundwater was high but decreased with longitudinal distance for all the GWTF cases. A study by Sharma *et al.* (2012) reported similar observations both for the fractured permeable and fractured impermeable formation.

It was observed that the increasing rate of WT fluctuation leads to an increase in the dissolved toluene mass recovery and can be helpful in the enhancement of advection processes with increasing hydraulic gradient, as shown in Figure 2. Also, in the GWTF-Rapid case, a high rate of WT and pore velocity fluctuations might have advected the solute mass entrapped in the microscopic immobile regions due to which a large amount of mass seeps out of these regions, finally resulting in the highest solute mass recovery as compared to the GWTF-Stable case. The magnitude of toluene mass recovered was found to decrease at a mild slope for the GWTF-Stable case, which can be seen in Figure 2(a) from the isoline intervals. However, for the GWTF-Rapid case, toluene mass recovered was found to decrease at a high gradient while moving away from the LNAPL source location, as depicted in Figure 2(b). It is hypothesized that the location or observation point with highest solute

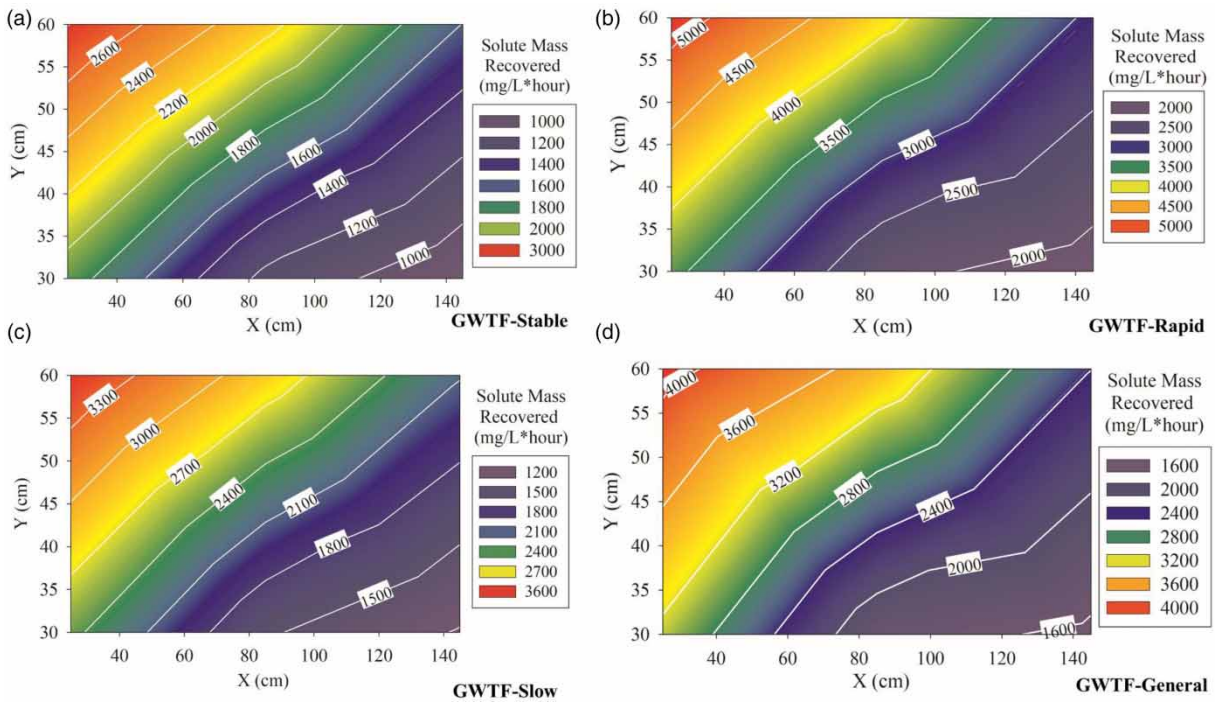

Figure 2 | The dissolved-phase toluene mass recovered for (a) GWTF-Stable, (b) GWTF-Rapid, (c) GWTF-Slow, and (d) GWTF-General.

mass recovered can be treated as a hot spot compared to other observation points, which need to be emphasized during remediation operations.

3.2. Mean residence time and variance

The variation of first temporal moment representing the mean residence time at various observation ports in the unsaturated and saturated regions for different GWTF scenarios is shown in Figure 3. Port numbers 1, 4, and 7 were placed in the unsaturated region (Figure 3(a)), while port numbers 8, 11, and 14 were placed in the saturated region (Figure 3(b)), with port-1 and port-8 located vertically below the LNAPL source, while port-7 and port-14 were placed at far away from source zone longitudinally. It should be noted that ports in the unsaturated region were placed ~30 cm below the LNAPL release port. Non-uniform variation of mean residence time with longitudinal direction was observed for all the considered cases in upper and lower locations of the variably saturated zone. The mean residence time of LNAPL solute for the GWTF-Stable case in the unsaturated region for all the ports was highest as compared to GWTF-Rapid, GWTF-Slow, and GWTF-General scenarios because the fluctuations (GWTF-Rapid, GWTF-Slow, and GWTF-General) in the WT and pore-water velocity advected the toluene from a particular location and reduced the residence time span with an increase in GWTF rate (Figure 3(a)). The toluene mass remains in the porous medium for a longer duration for port numbers 7 and 14, depicting the dominance of dispersion over advection at a location far away from LNAPL release port. Due to dominance of dispersion, plume spreading was higher at these locations (port numbers 7 and 14) as compared to ports at a shorter distance, which ultimately led to an enhanced mean residence time at larger travel distances. The value of mean residence time for the GWTF-Stable case in the saturated region was highest for the entire experimental duration, followed by GWTF-Slow, GWTF-General, and GWTF-Rapid (Figure 3(b)). The mean residence time for the top layer (unsaturated region) was found to be lower than the deep saturated layer, which might be caused by a higher biodegradation rate and a larger population of potential microbe in the unsaturated region to cause degradation. The port numbers 8–14, indicating the deep saturated layer of the tank, showed a low degradation rate with a smaller microbial population due to low oxygen levels. In this situation, toluene remains in the saturated region for a longer duration compared to the top layer having port numbers P1–P7, which causes a higher mean residence time.

Figure 4 shows the spatial variation of variance in the upper and lower layers of a 2D sand tank for different GWTF scenarios. The second temporal moment decreases non-linearly as we move away from a source location in both the unsaturated and saturated regions for all considered GWTF cases. In the top layer (unsaturated region), the variance of BTC varies from ~192 to ~93 h^2 for a 120 cm travel distance along the longitudinal direction, which is higher than the saturated region, where the second temporal moment varies from ~138 to ~38 h^2 for the GWTF-Rapid case. In all GWTF cases, second temporal

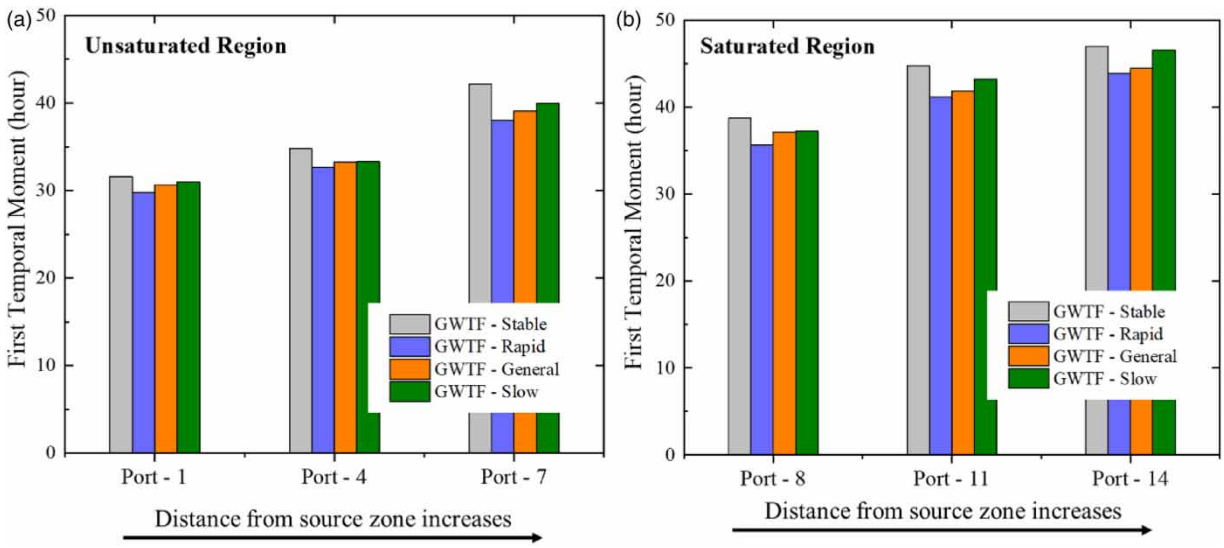

Figure 3 | Variations of first temporal moment in the (a) unsaturated and (b) saturated regions for various WT fluctuation scenarios.

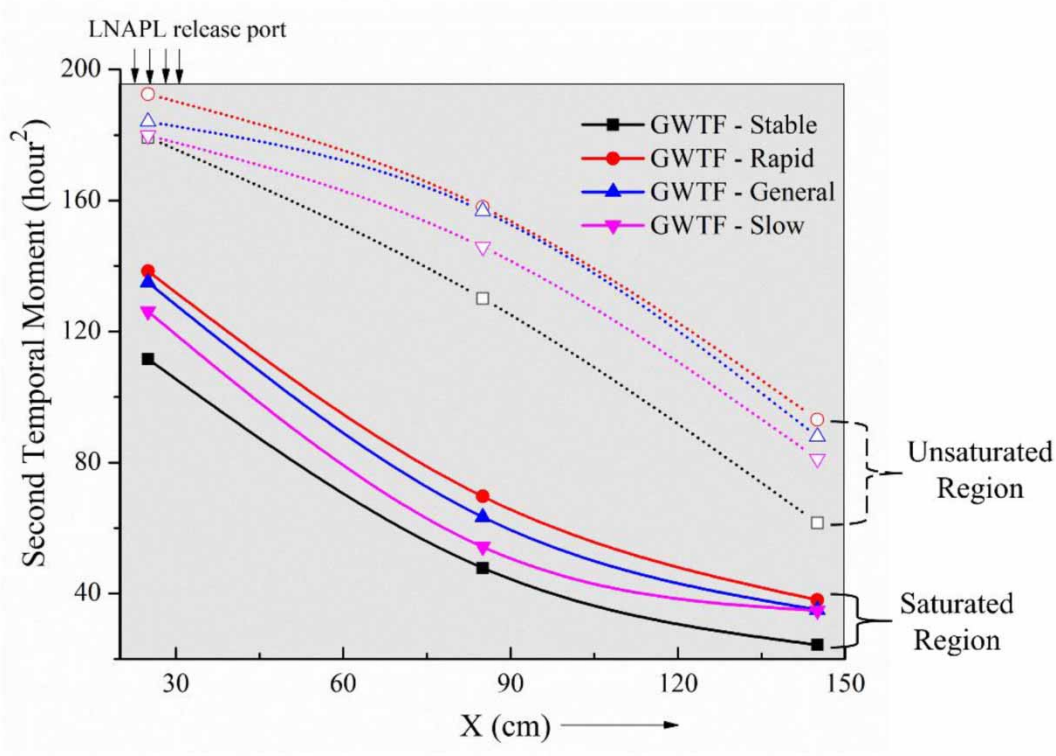

Figure 4 | Variations of second temporal moment for different WT fluctuation cases.

moments in the unsaturated region were observed to be higher than that of the saturated region. These findings were attributed to the higher amounts of variations in the advective fluxes in the unsaturated region in comparison to small variations in the saturated regions. The variation in the advective fluxes was mainly caused by variations in the pore-water velocity distribution in the unsaturated region compared to the saturated region.

The largest value of second temporal moment was observed for the GWTF-Rapid case in the top layer, depicting the strong variation of hydraulic conductivity field, which can be attributed to non-linear dependence of hydraulic conductivity and dispersion coefficient on moisture content level in the top layer. However, the lowest value of second temporal moment was observed for the GWTF-Stable case in the saturated region, which can be caused by anoxic conditions in the deeper saturated zone. Shorter mean residence time and larger variance of BTCs were observed in Figures 3 and 4 for a particular location, signifying the fast flow paths and dominance of advective transport. These observations are in-line with the findings of Blackmore *et al.* (2018) for contaminant transport experiments in waste rock piles. These similarities fortify the existence of microscale heterogeneity in the tank setup, though care was taken while packing the sand in the tank to create homogeneous conditions. It is also important to note that the mixing of end products via biodegradation of toluene may cause such variation in BTC, as this was a case of reactive transport.

Pearson's correlation coefficient was calculated for the first (T_1) and second temporal (T_2) moments for all GWTF scenarios. Statistical analysis of the first temporal moments revealed that the R^2 values for GWTF-Stable, GWTF-Rapid, GWTF-General, and GWTF-Slow cases were 0.983, 0.988, 0.982, and 0.987, as shown in Figure 5(a)–5(d). A similar trend for the second temporal moments can be observed in Figure 5(e)–5(h). The R^2 values of 0.977, 0.977, 0.956, and 0.959 were obtained for GWTF-Stable, GWTF-Rapid, GWTF-General, and GWTF-Slow cases. It can be observed that the first temporal moments from the HYDRUS-simulated concentrations matched the observed first temporal moments very well compared to the second temporal moments. Overall, the results of first and second temporal moments confirmed that the HYDRUS simulation of BTCs could capture the overall shapes of dissolved-phase toluene very closely. This type of analysis can be helpful in determining the overall deviation in the predicted solute concentrations.

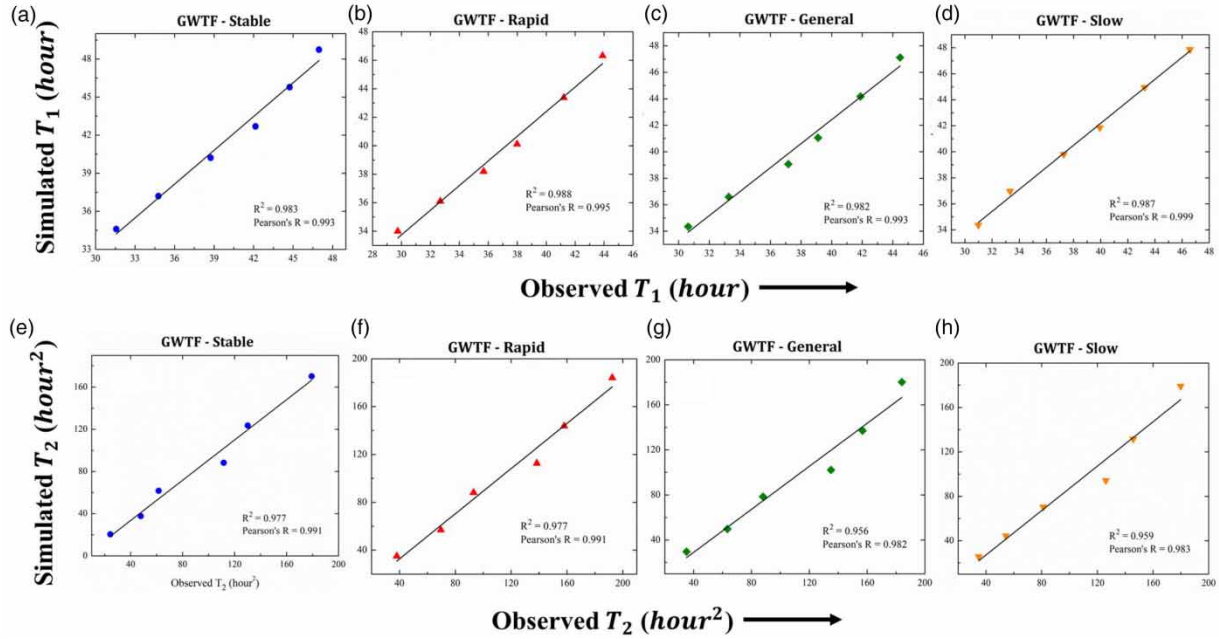

Figure 5 | Observed vs. simulated (a–d) first (T_1) and (e–h) second (T_2) normalized moments of the dissolved-phase toluene for all saturated and unsaturated locations.

Studies have reported the direct influence of WT fluctuations on the recovery rate of LNAPL (Wang *et al.* 2014; Teramoto *et al.* 2020). In the present study, the highest toluene mass recovery was observed under rapidly fluctuating WT conditions compared to slow (GWTF-Slow) and general (GWTF-General) cases. Similar findings of increased concentration of LNAPL dissolved-phase components due to WT fluctuations were reported for lab-scale (80 cm × 51 cm × 3.3 cm) aquifer conditions (Dobson *et al.* 2007). WT fluctuations caused an increase in biodegradation activity along with a dissolution of LNAPL components as compared to the model without fluctuation (Dobson *et al.* 2007). Not only the magnitude but the rate of WT fluctuation was observed as a governing factor controlling the spatiotemporal variation of LNAPL in the porous media (Oostrom *et al.* 2006). Similarly, in the present study, variation in the mass recovery and mean residence time was observed with several WT fluctuation scenarios, viz. GWTF-Rapid, GWTF-Slow.

In the study by Gupta *et al.* (2020), an increase in the microbial growth of hydrocarbon degraders was observed for fluctuating WT conditions in the column setup in comparison to static WT conditions. It is revealed that the WT fluctuation can act as a powerful tool for the remediation of NAPL-contaminated sites (Gupta *et al.* 2020). Similarly, the enhanced toluene mass recovery along with a decrease in the mean residence time was observed in the present study for the GWTF-Rapid case. Enhancement of the toluene mass recovery via manipulation of groundwater may help in reducing remediation costs and time. Also, an increase in the initial substrate concentration due to WT fluctuation will eventually help the remediation of contaminated sites governed by microbes. The quantification of the above findings via various temporal moments highlighted the significance of temporal moment-based approach and, thus, can be helpful in designing remediation strategies.

4. CONCLUSION

Hydrological interventions in the form of a dynamic groundwater act as a strong LNAPL removal tool. In this study, the ability of groundwater table manipulation has been tested to improve dissolved toluene mass from a plume zone. The study strongly supports the applicability of temporal moments to predict the time-averaged response of toluene plumes emanating from LNAPL pool in a soil–water system, which can be linked with management and remediation practices. The approach presented in the study would facilitate a monitoring campaign to determine sampling locations, operational parameters, etc., that can further support planning on the remediation strategies of various LNAPL-contaminated sites. However, there are a few limitations that could cause uncertainties in estimating temporal moments. The sensitivity analysis of the flow and

transport parameters using TMA was not implemented. In the future, the impact of low permeability regions such as silt/clay lenses on the plume evolution in the saturated porous media can be investigated using TMA. The implementation of TMA at field-scale conditions could be the next step to check the applicability of temporal moment-based approach. In conclusion, we strongly recommend that field managers manipulate the groundwater table dynamics by implementing pumping operations to improve the hydrocarbon mass recovery.

ACKNOWLEDGEMENTS

The authors are thankful to the Department of Science and Technology (DST), Government of India, for funding this research under the scheme of Ramanujan fellowship. The first author would like to acknowledge the Indian Institute of Technology, Delhi, for providing a Doctorate Fellowship. The authors are also thankful to the University Grant Commission, New Delhi, for providing a JRF/SRF for this study.

AUTHORS CONTRIBUTIONS

All authors contributed to the study conception and design. Material preparation, data collection and analysis were performed by A.G. and P.K.G. The first draft of the manuscript was written by A.G. and all authors commented on previous versions of the manuscript. The resource and mentorship were provided by S.C. and B.K.Y. All authors read and approved the final manuscript.

DATA AVAILABILITY STATEMENT

All relevant data are included in the paper or its Supplementary Information.

CONFLICT OF INTEREST

The authors declare there is no conflict.

REFERENCES

Basack, S., Goswami, G., Khabbaz, H. & Karakouzian, M. 2022 Flow characteristics through granular soil influenced by saline water intrusion: A laboratory investigation. *Civ. Eng. J.* **8**, 863–878. https://doi.org/10.28991/CEJ-2022-08-05-02.

Beegum, S., Šimůnek, J., Szymkiewicz, A., Sudheer, K. P. & Nambi, I. M. 2018 Updating the coupling algorithm between HYDRUS and MODFLOW in the HYDRUS package for MODFLOW. *Vadose Zo. J.* **17**, 180034. https://doi.org/10.2136/vzj2018.02.0034.

Blackmore, S., Smith, L., Ulrich Mayer, K. & Beckie, R. D. 2014 Comparison of unsaturated flow and solute transport through waste rock at two experimental scales using temporal moments and numerical modeling. *J. Contam. Hydrol.* **171**, 49–65. https://doi.org/10.1016/j.jconhyd.2014.10.009.

Blackmore, S., Pedretti, D., Mayer, K. U., Smith, L. & Beckie, R. D. 2018 Evaluation of single- and dual-porosity models for reproducing the release of external and internal tracers from heterogeneous waste-rock piles. *J. Contam. Hydrol.* **214**, 65–74. https://doi.org/10.1016/j.jconhyd.2018.05.007.

Chrysikopoulos, C. V. 1995 Three-dimensional analytical models of contaminant transport from nonaqueous phase liquid pool dissolution in saturated subsurface formations. *Water Resour. Res.* **31**, 1137–1145. https://doi.org/10.1029/94WR02780.

Dobson, R., Schroth, M. H. & Zeyer, J. 2007 Effect of water-table fluctuation on dissolution and biodegradation of a multi-component, light nonaqueous-phase liquid. *J. Contam. Hydrol.* **94**, 235–248. https://doi.org/10.1016/j.jconhyd.2007.07.007.

Ekeleme, A. C., Ekwueme, B. N. & Agunwamba, J. C. 2021 Modeling contaminant transport of nitrate in soil column. *Emerg. Sci. J.* **5**, 471–485. https://doi.org/10.28991/esj-2021-01290.

Essaid, H. I., Bekins, B. A. & Cozzarelli, I. M. 2015 Organic contaminant transport and fate in the subsurface: Evolution of knowledge and understanding. *Water Resour. Res.* **51**, 4861–4902. https://doi.org/10.1002/2015WR017121.

Fagerlund, F., Niemi, A. & Illangasekare, T. H. 2008 Modeling of nonaqueous phase liquid (NAPL) migration in heterogeneous saturated media: Effects of hysteresis and fluid immobility in constitutive relations. *Water Resour. Res.* **44**, 1–18. https://doi.org/10.1029/2007WR005974.

Garg, A., Leung, A. K. & Ng, C. W. W. 2015 Comparisons of soil suction induced by evapotranspiration and transpiration of S. heptaphylla. *Can. Geotech. J.* **52**, 2149–2155. https://doi.org/10.1139/cgj-2014-0425.

Garg, A., Li, J., Hou, J., Berretta, C. & Garg, A. 2017 A new computational approach for estimation of wilting point for green infrastructure. *Measurement* **111**, 351–358. https://doi.org/10.1016/j.measurement.2017.07.026.

Gaur, S., Omar, P. J., Eslamian, S., 2023 Advantage of grid-free analytic element method for identification of locations and pumping rates of wells. In: *Handbook of Hydroinformatics* (Eslamian, S. & Eslamian, F., eds). Elsevier, pp. 1–10. https://doi.org/10.1016/B978-0-12-821962-1.00003-9.

Goltz, M. & Huang, J. 2017 Method of moments. In: *Analytical Modeling of Solute Transport in Groundwater: UsingModels to Understand the Effect Of Natural Processes on Contaminant Fate and Transport*. (Goltz, M. & Huang, J., eds). John Wiley & Sons, Hoboken, New Jersey, pp. 87–120.

Govindaraju, R. S. & Das, B. S. 2007 *Moment Analysis for Subsurface Hydrologic Applications, Water Science and Technology Library*. Springer, Dordrecht, Netherlands. https://doi.org/10.1007/978-1-4020-5752-6.

Guleria, A., Swami, D., Sharma, A. & Sharma, S. 2019 Non-reactive solute transport modelling with time-dependent dispersion through stratified porous media. *Sadhana – Acad. Proc. Eng. Sci.* **44**, 81. https://doi.org/10.1007/s12046-019-1056-6.

Guleria, A., Swami, D., Joshi, N. & Sharma, A. 2020 Application of temporal moments to interpret solute transport with time-dependent dispersion. *Sādhanā* **45**, 159. https://doi.org/10.1007/s12046-020-01402-5.

Guo, Z., Fogg, G. E., Brusseau, M. L., LaBolle, E. M. & Lopez, J. 2019 Modeling groundwater contaminant transport in the presence of large heterogeneity: A case study comparing MT3D and RWhet. *Hydrogeol. J.* **27**, 1363–1371. https://doi.org/10.1007/s10040-019-01938-9.

Gupta, P. K. & Yadav, B. K. 2020 Three-dimensional laboratory experiments on fate and transport of LNAPL under varying groundwater flow conditions. *J. Environ. Eng.* **146**, 04020010. https://doi.org/10.1061/(ASCE)EE.1943-7870.0001672.

Gupta, P. K., Yadav, B. & Yadav, B. K. 2019 Assessment of LNAPL in subsurface under fluctuating groundwater table using 2D sand tank experiments. *J. Environ. Eng.* **145**, 04019048. https://doi.org/10.1061/(ASCE)EE.1943-7870.0001560.

Gupta, P. K., Gharedaghloo, B., Lynch, M., Cheng, J., Strack, M., Charles, T. C. & Price, J. S. 2020 Dynamics of microbial populations and diversity in NAPL contaminated peat soil under varying water table conditions. *Environ. Res.* **191**, 110167. https://doi.org/10.1016/j.envres.2020.110167.

Kim, J. & Corapcioglu, M. Y. 2003 Modeling dissolution and volatilization of LNAPL sources migrating on the groundwater table. *J. Contam. Hydrol.* **65**, 137–158. https://doi.org/10.1016/S0169-7722(02)00105-5.

Kleinknecht, S. M., Class, H. & Braun, J. 2017 Experimental study on retardation of a heavy NAPL vapor in partially saturated porous media. *Hydrol. Earth Syst. Sci.* **21**, 1381–1396. https://doi.org/10.5194/hess-21-1381-2017.

Naff, R. L. 1992 Arrival times and temporal moments of breakthrough curves for an imperfectly stratified aquifer. *Water Resour. Res.* **28**, 53–68. https://doi.org/10.1029/91WR02105.

Narayanan, M., Tracy, J. C., Davis, L. C. & Erickson, L. E. 1998a Modeling the fate of toluene in a chamber with alfalfa plants: 1. Theory and modeling concepts. *J. Hazard. Subst. Res.* **1**. https://doi.org/10.4148/1090-7025.1004.

Narayanan, M., Tracy, J. C., Davis, L. C. & Erickson, L. E. 1998b Modeling the fate of toluene in a chamber with Alfalfa plants: 2. Numerical results and comparison study. *J. Hazard. Subst. Res.* **1**. https://doi.org/10.4148/1090-7025.1005.

Nyakundi, R., Nyadawa, M. & Mwangi, J. 2022 Effect of recharge and abstraction on groundwater levels. *Civ. Eng. J.* **8**, 910–925. https://doi.org/10.28991/CEJ-2022-08-05-05.

Omar, P. J., Gaur, S., Dwivedi, S. B. & Dikshit, P. K. S. 2019 Groundwater modelling using an analytic element method and finite difference method: an insight into Lower Ganga river basin. *J. Earth Syst. Sci.* **128**, 195. https://doi.org/10.1007/s12040-019-1225-3.

Omar, P. J., Gaur, S., Dwivedi, S. B. & Dikshit, P. K. S. 2020 A modular three-dimensional scenario-based numerical modelling of groundwater flow. *Water Resour. Manage.* **34**, 1913–1932. https://doi.org/10.1007/s11269-020-02538-z.

Omar, P. J., Gaur, S. & Dikshit, P. K. S. 2021 Conceptualization and development of multi-layered groundwater model in transient condition. *Appl. Water Sci.* **11**, 162. https://doi.org/10.1007/s13201-021-01485-3.

Oostrom, M., Hofstee, C. & Wietsma, T. W. 2006 LNAPLs do not always float: An example case of a viscous LNAPL under variable water table conditions. In: *26th Annual American Geophysical Union Hydrology Days*. https://doi.org/AC05-76RL01830.

Pang, L., Goltz, M. & Close, M. 2003 Application of the method of temporal moments to interpret solute transport with sorption and degradation. *J. Contam. Hydrol.* **60**, 123–134. https://doi.org/10.1016/S0169-7722(02)00061-X.

Sharma, P. K., Sekhar, M., Srivastava, R. & Ojha, C. S. P. 2012 Temporal moments for reactive transport through fractured impermeable/permeable formations. *J. Hydrol. Eng.* **17**, 1302–1314. https://doi.org/10.1061/(ASCE)HE.1943-5584.0000586.

Sharma, A., Swami, D., Joshi, N., Kartha, S., Chandel, A. & Guleria, A. 2020 Study of dynamic concentration gradient on mass transfer coefficient: New approach to mobile–immobile modeling. *J. Hazardous, Toxic, Radioact. Waste* **24**, 04020036. https://doi.org/10.1061/(ASCE)HZ.2153-5515.0000523.

Šimůnek, J., van Genuchten, M. T. & Šejna, M. 2006 *The HYDRUS Software Package for Simulating the Two- and Three-Dimensional Movement of Water, Heat, and Multiple Solutes in Variably-Saturated Media*. Prague, Czech Republic.

Šimůnek, J., van Genuchten, M. T. & Šejna, M. 2016 Recent developments and applications of the HYDRUS computer software packages. *Vadose Zo. J.* **15**. vzj2016.04.0033. https://doi.org/10.2136/vzj2016.04.0033.

Singh, D., Roy, S., Pant, H. J. & Phirani, J. 2021 Solid-fluid interfacial area measurement for wettability quantification in multiphase flow through porous media. *Chem. Eng. Sci.* **231**, 116250. https://doi.org/10.1016/j.ces.2020.116250.

Singh, D., Roy, S., Pant, H. J. & Phirani, J. 2022 A novel approach for wettability estimation in geological systems by fluid–solid interfacial area measurement using tracers. *J. Pet. Sci. Eng.* **215**, 110722. https://doi.org/10.1016/j.petrol.2022.110722.

Teramoto, E. H., Pede, M. A. Z. & Chang, H. K. 2020 Impact of water table fluctuations on the seasonal effectiveness of the pump-and-treat remediation in wet–dry tropical regions. *Environ. Earth Sci.* **79**, 435. https://doi.org/10.1007/s12665-020-09182-1.

U.S.EPA 2006 *In Situ and Ex Situ Biodegradation Technologies for Remediation of Contaminated Sites*. US of Research, Office Transfer Support Division, Technology Grosse, Douglas.

Wang, W., Kuo, T., Chen, Y., Fan, K., Liang, H. & Chen, J. 2014 Effect of precipitation on LNAPL recovery performance: an integration of laboratory and field results. *J. Pet. Sci. Eng.* **116**, 1–7. https://doi.org/10.1016/j.petrol.2014.03.001.

Yadav, B. K., Shrestha, S. R. & Hassanizadeh, S. M. 2012 Biodegradation of toluene under seasonal and diurnal fluctuations of soil–water temperature. *Water, Air, Soil Pollut.* **223**, 3579–3588. https://doi.org/10.1007/s11270-011-1052-x.

First received 17 October 2022; accepted in revised form 13 March 2023. Available online 29 March 2023